Theoretical Study on CO_2 Hydrogenation Mediated by Ru-PNP Pincer Complexes: An Implication Towards Rational Catalyst Design

Shahnaz S. Rohman, Chayanika Kashyap, Amlan J. Kalita, Sabnam S. Ullah, Indrani Baruah, Lakhya J. Mazumder and Ankur K. Guha*

Advanced Computational Chemistry Centre, Cotton University, Panbazar, Guwahati, Assam, INDIA-781001

*Email: ankurkantiguha@gmail.com

ABSRTACT

Catalytic CO_2 reduction mediated by Ru-PNP pincer complexes has been studied using density functional theory (DFT). Calculations clearly reveal that modification of the PNP pincer framework by introducing planar conjugation in the backbone improves the catalytic efficiency. Activation strain model reveals that reduction of strain in the transition states with modified PNP framework associated with the insertion of CO_2 molecule is responsible for lowering the activation barrier. Calculations also reveal that electron withdrawing substituents at the PNP ligand improves the catalytic performance.

Keywords: CO_2 reduction, theoretical calculations, conjugation, substituent.

INTRODUCTION

The increasing concentration of carbon dioxide in the atmosphere has intensified the need for its proper utilization as a non toxic carbon source in clean energy technologies. Carbon dioxide is not only found to be an economical and renewable carbon source, but also serves as an important C_1 building block for many chemicals.[1] Besides contributing in the sustainable development of chemical industry, products like formic acid or methanol also behave as potential hydrogen storage agents.[2,3] As such, hydrogenation of CO_2 has grabbed

immense interest of researchers and its efficient conversion has turned out to be a subject of numerous studies.

Bio-relevant metals viz. Fe[4,5,6,7]and Co[8,9,10] have been used in homogenous systems to catalyse the reaction of hydrogenation but reports show that use of noble metals including Rh[11,12], Ir [13,14] and Ru[15-18] make the process even more efficient. Nozaki and co workers introduced an Ir based PNP pincer complex for CO_2 hydrogenation and forwarded two competing pathways — ligand dearomatization and hydrogenolysis.[19] The iridium (III) trihydride catalyst was reported to exhibit highest catalytic activity in aqueous KOH. While reversibility of this reaction was favoured when triethanolamine was used.[20] Later on, theoretical reports of Yang[8] and Ahlquist[21] confirmed that base assisted H—H cleavage mechanism was energetically more favourable. The use of Ru-PNP and PNN pincer complexes in recent times have shown promises towards the catalytic process.[22] These complexes reversibly bind CO_2 forming 1,3- CO_2 adducts. Huff and Sanford used PNN pincer ligands and reported a TOF of 2200 h^{-1}.[23,24] Filonenko *et al*. have shown that metal-ligand cooperation in Ru-PNP complexes lowers the efficiency of the catalytic reaction.[25a]

With the advancement of computational tools, the design of new catalysts is making promising progress.[26-30] Inspired by the performances of Ru-PNP pincer complexes,[15-18,25] herein, we intend to investigate the effect of substituents on the PNP ligand and skeletal modification of the PNP ligand. As substituents have a profound effect on many catalytic processes,[18,31] this study is aimed to provide better understanding towards rationale catalysts design. In this study, three Ru-catalysts including the modified PNP framework of the ligand (**1a**, **1b** and **1c**, Scheme 1) are considered and the energetic of the catalytic process has been elucidated. In addition, calculations have been performed to illustrate the effect of electron withdrawing $-CF_3$ and electron donating $-CH_3$ substituents towards the efficacy of the

catalysts. On the basis of detailed calculations and analysis, Ru-PNP catalysts **1b** and **1c** with a more rigid PNP skeleton are proposed to be promising catalysts for CO_2 reduction. Electron withdrawing substituent $–CF_3$ has been found to increase the efficacy of all these catalysts.

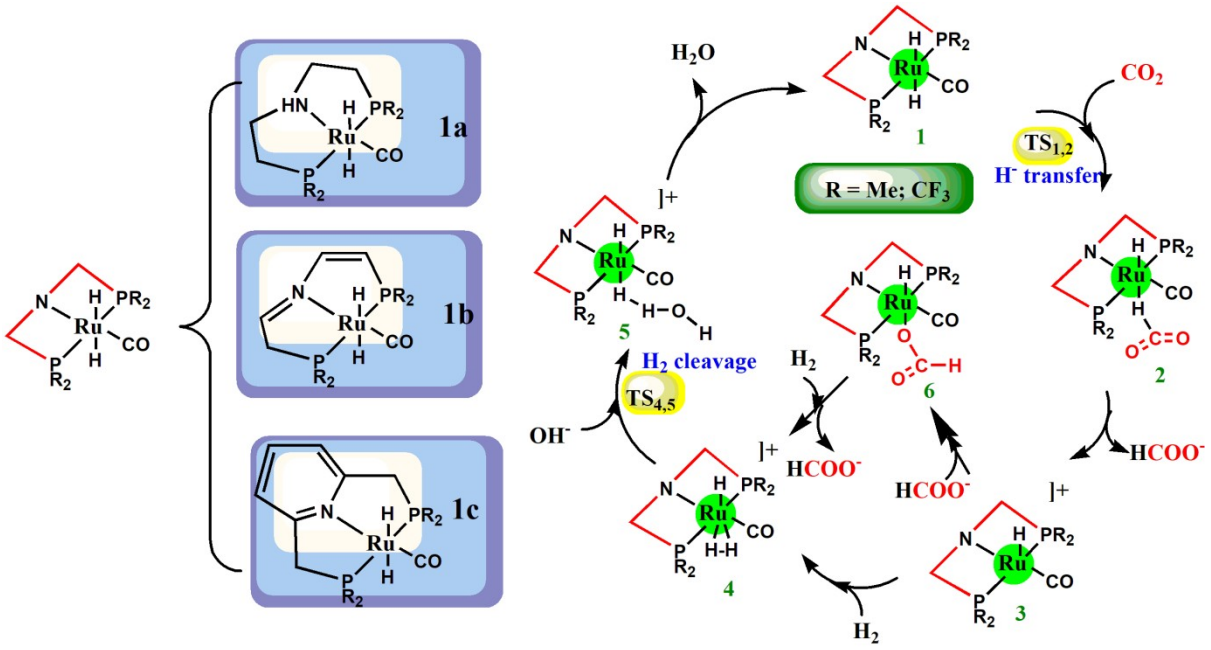

Scheme 1. The catalytic cycle for CO_2 hydrogenation and the three catalysts (**1a**, **1b** and **1c**) with different type of PNP ligand frameworks considered for this study.

COMPUTATIONAL DETAILS

All the geometries were fully optimized without any symmetry constraints using meta-GGA based M06-2X functional[32] and 6-311+G** basis set[33] for main group atoms. Stuttgart/Dresden effective core potential (ECP)[34] basis set was employed for the transition metal Ru. Choice of the level of theory is based on the comparison of the experimental structural parameters of **1a** with calculated ones. The calculated values are found to be in good agreement with the experimental parameters (S1, Supporting Information). Harmonic vibrational frequencies were calculated to confirm the nature of transition states (one imaginary frequency) and intermediates (all frequencies are real). The transition states were further verified by intrinsic reaction coordinate (IRC) analysis at the same level of theory.[35]

Solvent correction was taken into account by performing all the calculations in tetrahydrofuran (THF) medium using polarizable continuum model (PCM)[36] during optimization as well as vibrational frequency calculations. All energies are zero point and thermal corrected. Natural bond orbital (NBO)[37] analyses were also performed to understand the electronic feature of the systems. All calculations were performed using Gaussian 16 suite of programs.[38]

RESULTS AND DISCUSSION

Overview of the Catalytic Cycle. Before discussing skeletal and electronic modification of the catalyst, we wish to explain several important feature of the catalytic cycle.[13,22,25] As shown in Scheme 1, the mechanism of CO_2 hydrogenation is speculated to initiate with bis-hydrido Ru-PNP complex **1** which is subjected to CO_2 addition. It should be noted that a detailed mechanistic study by Filonenko *et. al.* have shown that bis-hydrido Ru-PNP complex **1** provides the unique lowest energy barrierless pathway of CO_2 hydrogenation.[25b] For the sake of brevity, the geometrical changes during the CO_2 hydrogenation is shown in Fig 1 for catalyst **1a-Me** only and the energetic for **1a-1c** with R = Me is shown in Fig 2.

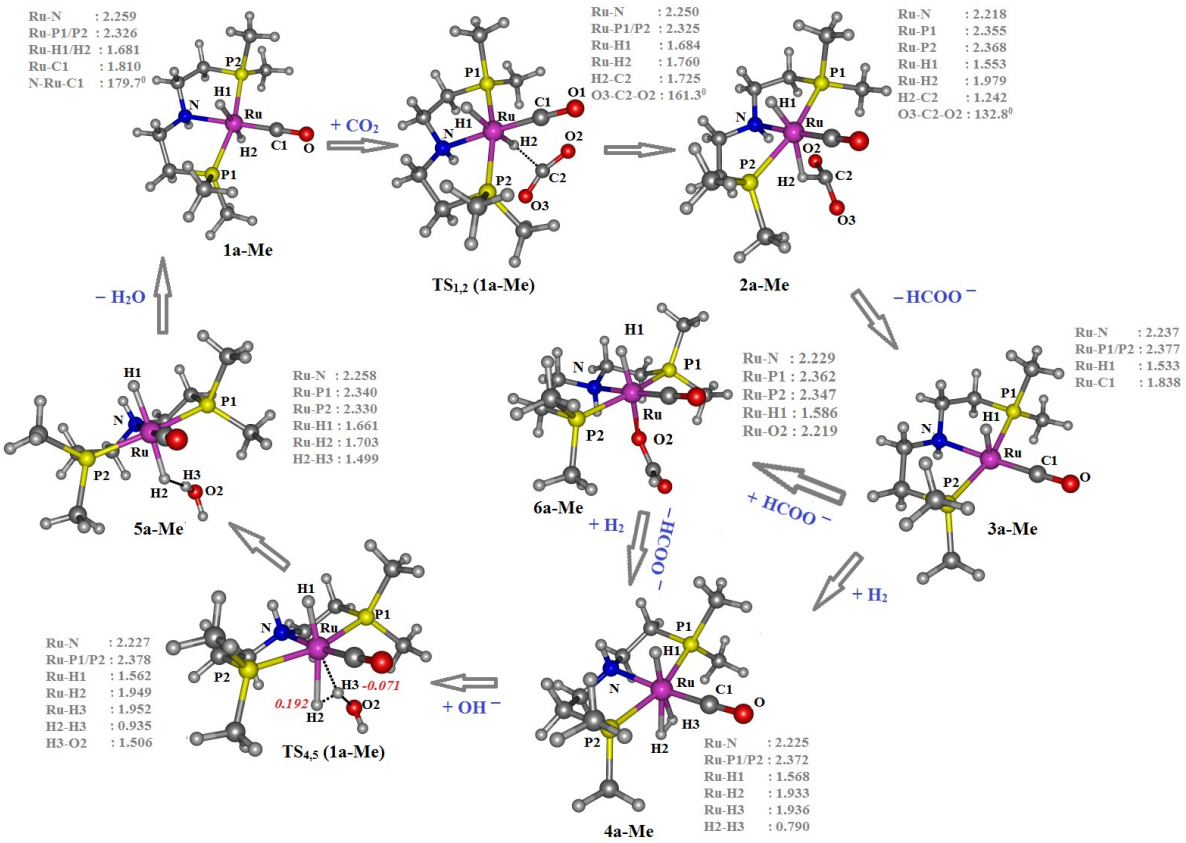

Fig 1. Geometric changes during CO_2 hydrogenation by **1a**. Bond lengths are in Å and angles are in degrees. Natural charges (in *e*) at H2 and H3 in **$TS_{4,5}$ (1a-Me)** are shown in red italic font.

CO_2 molecule attacks the hydridic H attached to the Ru centre to form H-bound formate complex **2a-Me** via **$TS_{1,2}$ (1a-Me)** in which the distance between the Ru bound H and C atom of CO_2 (H2-C2) is 1.725Å (Fig 1). Geometries of **$TS_{1,2}$ (1b-Me)** and **$TS_{1,2}$ (1c-Me)** are shown in Fig 3. The H2-C2 distances in **$TS_{1,2}$ (1b-Me)** and **$TS_{1,2}$ (1c-Me)** are 1.625 and 1.746 Å. The Ru-H2 distance (1.916Å) is most elongated in **$TS_{1,2}$ (1c-Me)** (Fig 3). The CO_2 molecule becomes slightly bent in **$TS_{1,2}$**. The barrier height for this step lies in the range of 9.2—23.4 kcalmol^{-1} (Fig 2) and is lowest for **1c**. The formate complex **2** then decomposes into a five coordinated complex **3** by liberating formate anion $HCOO^-$. This might be followed either by re-addition of $HCOO^-$ to form an O-bound formate complex **6** which may

undergo ligand exchange to further generate **4** or by H_2 addition to the metal centre leading directly to a Ru-dihydrogen complex **4**. The formation of the O-bound complex **6** is found to be slightly more feasible than that of **4** in all the three cases. This is also in tune with previous theoretical calculations on the mechanistic pathway mediated by Fe, Co and Ir-PNP pincer complexes.[8] The H_2 molecule in **4** binds in η^2 fashion to the Ru centre. On introducing the base (OH^-), complex **4** undergoes heterolytic H-H cleavage via $\mathbf{TS_{4,5}}$ (Fig 1 and 3) to release an H_2O molecule and thereby regenerating the bis-hydrido Ru-PNP complex **1**. The computed natural charges at the H atoms of η^2 bound H_2 are respectively -0.071e and 0.192e in $\mathbf{TS_{4,5}}$ **(1a-Me)**, -0.063e and 0.187e in $\mathbf{TS_{4,5}}$ **(1b-Me)** and -0.069e and 0.190e in $\mathbf{TS_{4,5}}$ **(1c-Me)** and thus supporting the heterolytic cleavage of the η^2 bound H_2.

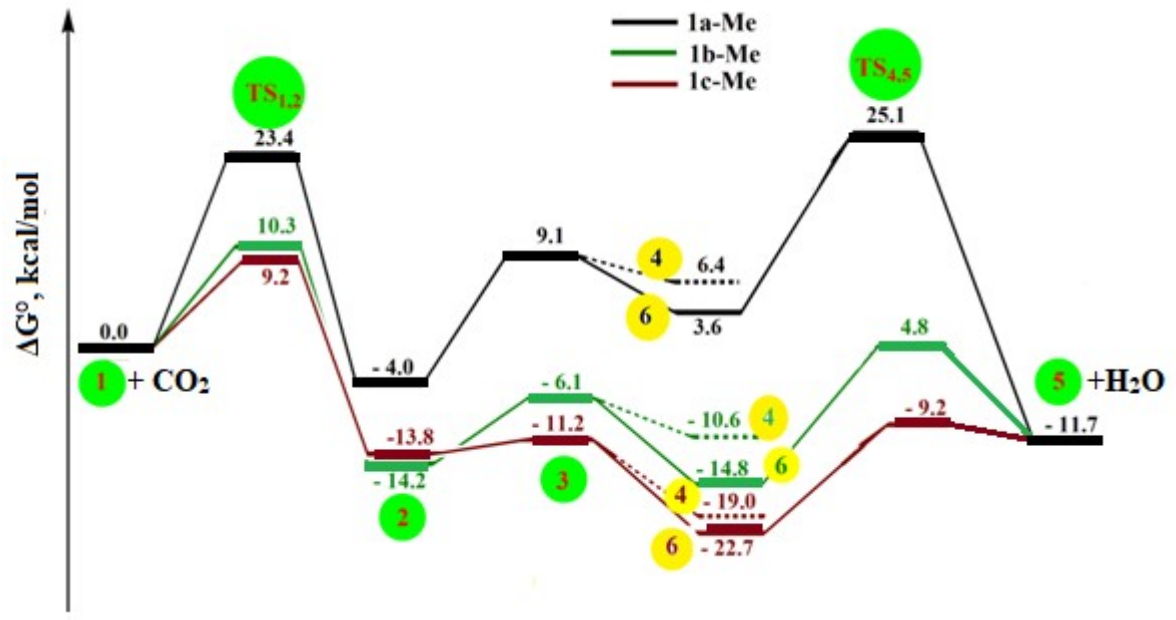

Fig 2. The energy profile diagram for CO_2 hydrogenation of methyl substituted catalysts (**1a-Me**, **1b-Me** and **1c-Me**).

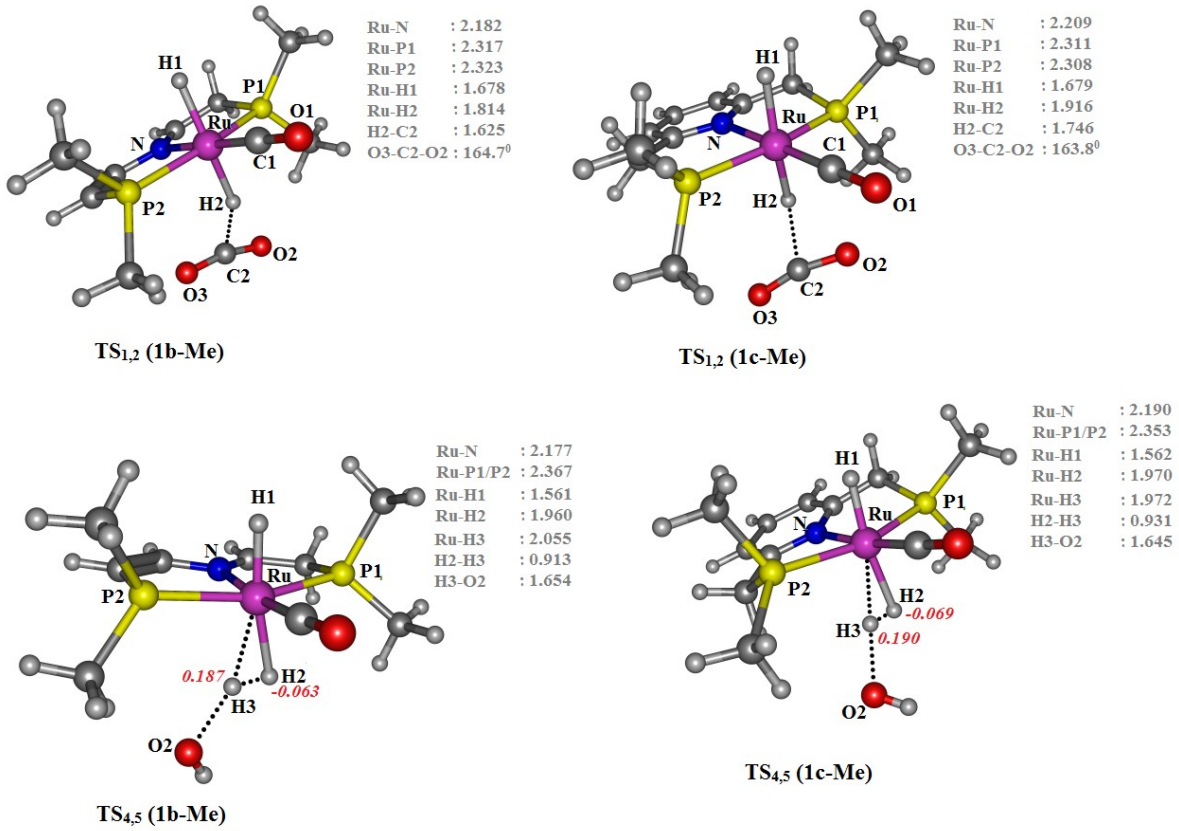

Fig 3. Optimized geometries of **$TS_{1,2}$ (1b-Me)**, **$TS_{1,2}$ (1c-Me)**, **$TS_{4,5}$ (1b-Me)** and **$TS_{4,5}$ (1b-Me)**. Bond lengths are in Å and angles are in degrees. Natural charges (in *e*) at H2 and H3 are shown in red italic font.

The energy profile diagram (Fig 2) clearly shows that the energy barriers for catalyst **1a** is significantly higher than that of **1b** and **1c** which suggests that **1b** and **1c** are more efficient for CO_2 hydrogenation. To investigate the probable reason behind the lower activation barrier with **1b** and **1c**, we first employed the activation strain model of chemical reactivity introduced by Bickelhaupt *et. al.*[39,40] This model is a fragment based approach and would give us an insight of the effect of various ligand frameworks on the activation barriers involved in CO_2 reduction. According to this model the activation energy of a reaction may be decomposed into activation strain, $\Delta E^{\ddagger}_{strain}$ and TS interaction, $\Delta E^{\ddagger}_{int}$ (Eq. 1)

$$\Delta E^{\ddagger} = \Delta E^{\ddagger}_{strain} + \Delta E^{\ddagger}_{int}$$

$\Delta E^{\ddagger}_{strain}$ is the deformation energy required for the deformation of reactants from their equilibrium geometry to the geometry they acquire in the activated complex and $\Delta E^{\ddagger}_{int}$ is the interaction energy between the deformed reactants in the transition state.

The calculated $\Delta E^{\ddagger}_{strain}$ for the first step of the catalytic cycle i.e. the attack of CO_2 at the H−Ru bond indicates that the activation strain increases in the order **1c** < **1b** <**1a** (Fig 4). The deformation energy for **1a** is very high compared to **1b** and **1c** which may be attributed to the greater rigidity in the PNP framework in **1b** and **1c**. Hence, tuning the PNP framework towards more rigidity by introducing double bonds or pyridine like backbone may turn out to be a good modification of the catalyst. Filonenko *et. al* have previously demonstrated that pyridine-based Ru-PNP pincer complexes show superior catalytic performances towards reversible CO_2 hydrogenation.[25]

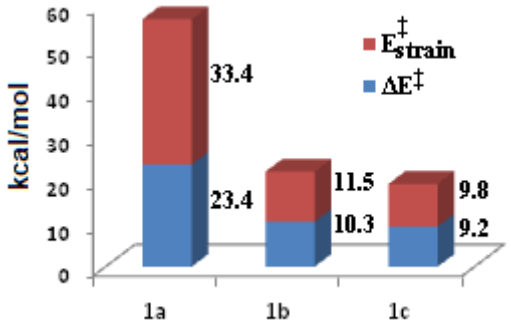

Fig 4. Variation of activation strain energy $\Delta E^{\ddagger}_{strain}$ with activation energy $\Delta E^{\ddagger}$.

We further used energy decomposition analysis (EDA)[42] of the transition states involved in the first step, i, e., the CO_2 insertion step, to have an idea of the energetic contribution. Various methods have been put forward to characterize the changes in reactivity and structures of reactants during the course of a reaction, EDA is one such elegant approach.[42] This scheme was confined to structures that correspond to minima on potential energy surfaces until 2011 when Mitoraj *et. al* applied the same to investigate the changes in electronic structures of reactants along the reaction path which includes even saddle points.[43] Here we have performed EDA to quantify various components of interaction energy in $\mathbf{TS_{1\text{-}2}}$ (**1a-Me**, **1b-Me** and **1c-Me**) that prevails between the key fragments i.e., the methyl substituted Ru-catalyst (**1a, 1b and 1c**) and CO_2 molecule. The total energy variation of forming a complex can be decomposed as

$$\Delta E_{tot} = E^{complex} - \sum_i E_i^{frag} = (¿\Delta E_{els} + \Delta E_{Ex}) + \Delta E_{orb} = \Delta E_{steric} + \Delta E_{polar} ¿$$

where ΔE_{els} is electrostatic interaction term, normally negative if the two fragments are neutural; $\Delta E_{Ex}$is exchange repulsion term, which comes from the Pauli repulsion effect and is invariably positive. For convenience, it is customary to combine these two terms as steric term (ΔE_{steric}). ΔE_{orb} in above formula is orbital interaction term, and sometimes also known as induction term or polarization term. ΔE_{orb} arises from the mix of occupied MOs and virtual MOs. If the combined wavefunction is used as initial guess for complex, then E_{orb} can be evaluated by subtracting the first SCF iteration energy from the last SCF iteration energy. All these calculations were performed using a combination of Gaussian[38] and Multiwfn suite of program.[41]

$$\Delta E_{orb} = E_{SCF,last} - E_{SCF,1st}$$

Table 1 contains the numerical data of the energy decomposition analysis. ΔE_{els} and ΔE_{orb} are the stabilizing terms while ΔE_{Ex} is the destabilizing component. It is evident from Table 1 that all these molecules have significant electrostatic attraction and the corresponding term has maximum contribution towards the interaction energy. Both the orbital and electrostatic contribution together overcompensates the exchange energy and is found to increase quantitatively down the column from **1a-Me** to **1c-Me**. This gives a clear indication that electrostatic attraction is dominant over orbital overlap in the transition states. The decreasing barrier height down the column can also be attributed to increase in extent of stabilizing factors i.e. ΔE_{els} and ΔE_{orb}.The repulsive component which is the result of interactions between the occupied orbitals ΔE_{Ex} is significantly smaller and contributes almost equally in all the systems.

Table 1. The EDA terms for $\mathbf{TS_{1,2}}$ with Me substituent. All energies are in kcal/mol.

Molecule	ΔE_{Ex}	ΔE_{els}	ΔE_{orb}	ΔE_{tot}
$TS_{1,2}$ (1a-Me)	2.1	-5.3	-2.9	-6.1
$TS_{1,2}$ (1b-Me)	2.3	-6.1	-3.2	-7.0
$TS_{1,2}$ (1c-Me)	2.3	-7.3	-4.1	-9.1

Effect of Electron Withdrawing Substituent. So far we have discussed the effect of different PNP framework on the activity of the Ru catalyst. We now turn our attention to investigate the effect of electron withdrawing substituent $–CF_3$ on the catalytic performance. Before discussing the effect of substituents, the elucidation of the electronic process of the catalytic cycle is very essential. We investigated the population changes along the intrinsic reaction coordinate (IRC)[35] in the first step, i, e,. CO_2 insertion step (Fig 5) as it is the most important step of the catalytic cycle.[25] We used **1a-Me** for this analysis and discussion considering it to be the standard. Fig 5 reveals that during the first step of CO_2 insertion the electron population of CO_2 decreases on going from **1a-Me** to **2a-Me**. However, the electron population of Ru and H increases during the reaction. This is a clear indication of charge transfer from CO_2 to H. Therefore, electron withdrawing substituent like $–CF_3$ attached to P atom of the PNP ligand will make the Ru centre electron poor and thereby expected to increase the charge flow from CO_2 to Ru through the H atom. This in turn is expected to stabilize the transition state $\mathbf{TS_{1,2}}$ **(1a-Me)** and thereby, facilitates the catalytic performance. Indeed, replacement of $–CH_3$ by $–CF_3$ at the P atom of PNP ligand decreases the barrier dramatically for all the catalysts (Fig 6) and thereby increases the catalytic activity.

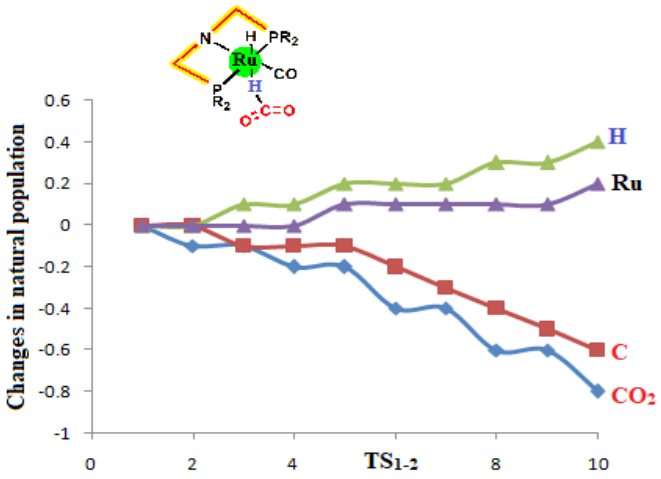

Fig 5. Natural population changes (in |e|) on coordination of CO_2 to the catalyst **1a-Me**. Positive values represent increase in population and vice-versa.

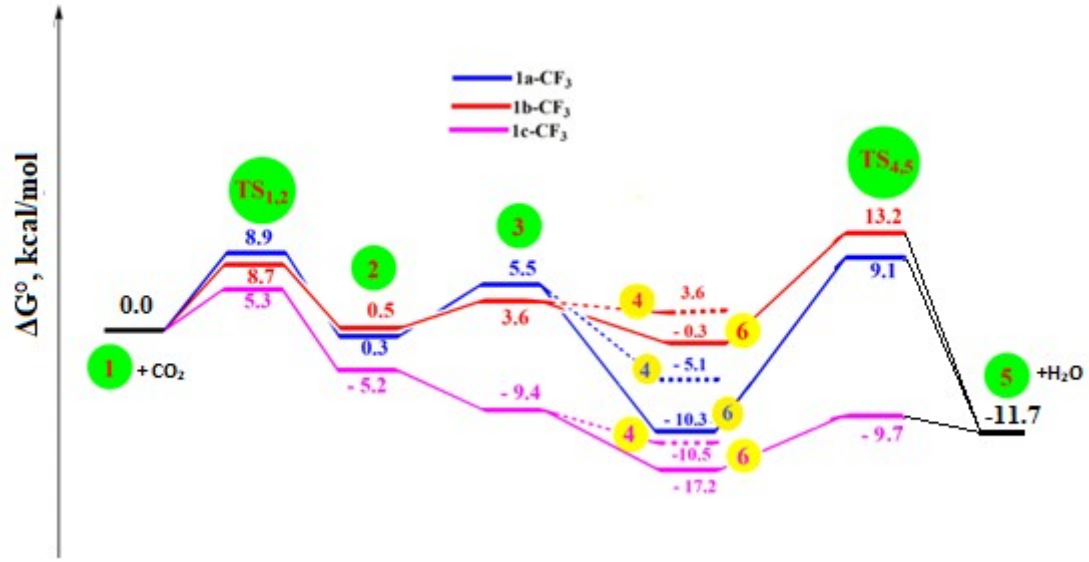

Fig 6. Energy profile diagram for the catalytic cycle with —CF_3 substituted catalysts (**1a-F, 1b-F and 1c-F**).

CONCLUSIONS

Density functional calculations were carried out to discuss the mechanism of CO_2 reduction using Ru-PNP complexes and to study the elementary steps involved in the catalytic cycle. Three different catalysts consisting of different PNP ligands were considered in this study. Energetic of the reaction profile reveals that catalyst **1b** and **1c** with planar conjugation and pyridine based PNP ligand are more efficient towards CO_2 reduction. Activation strain model reveals that there is reduction in strain for **1b** and **1c** in the transition states for the CO_2 insertion step. Energy decomposition analysis further confirmed the presence of greater contribution of electrostatic component towards the stabilizing energy in

case of **1b** and **1c**. Analysis of the electronic process reveals that there is significant charge transfer from CO_2 to the H atom attached to Ru centre and therefore, incorporation of electron withdrawing —CF_3 substituent further lowers the activation barrier of the CO_2 insertion step.

ASSOCIATED CONTENT

Fig S1 and Cartesian coordinates of all the optimized geometries.

ACKNOWLEDGEMENT

A. K. G. acknowledges Science and Engineering Research Board, (SERB), Department of Science and Technology (DST), India for the financial grant (ECR/2016/001466).

REFERENCES

1. K. Huang, C. L. Sun, Z. J. Shi, Chem. Soc. Rev. 40 (2011) 2435.
2. M. Nielsen, E. Alberico, W. Baumann, H. J. Drexler, H. Junge, S. Gladiali, M. Beller, Nature 495 (2013) 85.
3. S. Enthaler, ChemSusChem. 1 (2008) 801.
4. C. Federsel, A. Boddien, R. Jackstell, R. Jennerjahn, P. J. Dyson, R. Scopelliti, G. Laurenczy, M. Beller, Angew. Chem. Int. Ed. 49 (2010) 9777.
5. A. Boddien, D. Mellmann, F. Gärtner, R. Jackstell, H. Junge, P. J. Dyson, G. Laurenczy, R. Ludwig, M. Beller, Science 333 (2011) 1733.
6. R. Langer, Y. Diskin−Posner, G. Leitus, L. J. Shimon, Y. Ben−David, D. Milstein, Angew. Chem. Int. Ed. 50 (2011) 9948.
7. X. Yang, Inorg. Chem. 50 (2011) 12836.
8. X. Yang, ACS Catal. 1 (2011) 849.
9. C. Federsel, C. Ziebart, R. Jackstell, W. Baumann, M. Beller, Chem. Eur. J. 18 (2012) 72.
10. M. S. Jeletic, M. T. Mock, A. M. Appel, J. C. Linehan, J. Am. Chem. Soc. 135 (2013) 11533.
11. Y. Himeda, S. Miyazawa, T. Hirose, ChemSusChem. 4 (2011) 487.
12. D. Bonincontro, E. A. Quadrelli, *Rhodium Catalysis* Springer, Cham. 2016, pp 263−282.
13. T. J. Schmeier, G. E. Dobereiner, R. H. Crabtree, N. Hazari, J. Am. Chem. Soc. 133 (2011) 9274.

14. G. F.Manbeck, K. Garg, T. Shimoda, D. J. Szalda, M. Z. Ertem, J. T. Muckerman, E. Fujita, Faraday Discuss. 198 (2017) 301－317.
15. C. Yin, Z. Xu, S. Y. Yang, S. M. Ng, K. Y. Wong, Z. Lin, C. P. Lau, Organometallics 20 (2001) 1216.
16. Y. Gao, J. K. Kuncheria, H. A. Jenkins, R. J. Puddephatt, G. P. Yap, J. Chem. Soc., Dalton Trans. 18 (2000) 3212.
17. J. Elek, L. Nádasdi, G. Papp, G. Laurenczy, F. Joó, Appl. Catal. A: Gen. 255 (2003) 59.
18. Y. Y. Ohnishi, T. Matsunaga, Y. Nakao, H. Sato, S. Sakaki, J. Am.Chem. Soc. 127 (2005) 4021.
19. R. Tanaka, M. Yamashita, K. Nozaki, J. Am. Chem. Soc. 131 (2009) 14168.
20. R. Tanaka, M. Yamashita, L. W. Chung, K. Morokuma, K. Nozaki, Organometallics 30 (2011) 6742.
21. M. S. Ahlquist, J. Mol. Catal. A: Chem. 324 (2010) 3.
22. J. I. van der Vlugt, J. N. Reek, Angew. Chem. Int. Ed. 48 (2009) 8832.
23. C. A. Huff, M. S. Sanford, J. Am. Chem. Soc. 133 (2011) 18122.
24. C. A. Huff, M. S. Sanford, ACS Catal. 3 (2013) 2412.
25. (a) G. A. Filonenko, M. P. Conley, C. Copéret, M. Lutz, E. J. Hensen, E. A. Pidko, ACS Catal. 3 (2013) 2522. (b) G. A. Filonenko, E. J. Hensen, E. A. Pidko, Catal. Sci. Technol. 4 (2014) 3474. (c) G. A. Filonenko, R. van Putten, E. N. Schulpen, E. J. M. Hensen, E. A. Pidko, ChemCatChem, 6 (2014) 1526; (d) S. Kar, R. Sen, J. Kothandaraman, A. Goeppert, R. Chowdhury, S. B. Munoz, R. Haiges, G. K. S. Prakash, J. Am. Chem. Soc. 141 (2019) 3160.
26. J. B. Siegel, A. Zanghellini, H. M. Lovick, G. Kiss, A. R. Lambert, J. L. Clair, St. J. L. Gallaher, D. Hilvert, M. H. Gelb, B. L. Stoddard, K. N. Houk, F. E. Michael, D. Baker, Science 329 (2010) 309.
27. J. K. Nørskov, T. Bligaard, J. Rossmeisl, C. H. Christensen, Nat. Chem. 1 (2009) 37.
28. K. N. Houk, P. H. Y Cheong, Nature 455 (2008) 309.
29. M. Hölscher, W. Leitner, Chem. Eur. J. 16 (2010) 14266.
30. G. Lu, H. Li, L. Zhao, F. Fang Huang, P. v. R. Schleyer, Z. –X. Wang, Chem. Eur. J. 17 (2011) 2038.
31. G. Zeng, S. Maeda, T. Taketsugu, S. Sakaki, ACS Catal. 6 (2016) 4859.
32. Y. Zhao, D. G. Truhlar, Theor. Chem. Acc. 120 (2008) 215.

265 33. V. A. Rassolov, J. A. Pople, M. A. Ratner, T. L. Windus, J. Chem. Phys. 109 (1998)
266 1223.
267 34. P. Fuentealba, H. Preuss, H. Stoll, L. Von Szentpály, Chem. Phys. Lett. 89 (1982)
268 418.
269 35. (a) C. Gonzalez, B. H. Schlegel, J. Chem. Phys. 90 (1989) 2154. (b) C. Gonzalez, B.
270 H. Schlegel, J. Phys. Chem. 94 (1990) 5523.
271 36. E. L. Coitiño, J. Tomasi, R. Cammi, J. Comp. Chem. 16 (1995) 20.
272 37. E. D. Glendening, C. R. Landis, F. Weinhold, J. Comp. Chem. 34 (2013) 1429.
273 38. Gaussian 16, Revision A.03, M. J. Frisch, G. W. Trucks, H. B. Schlegel, G. E.
274 Scuseria, M. A. Robb, J. R. Cheeseman, G. Scalmani, V. Barone, G. A. Petersson, H.
275 Nakatsuji, X. Li, M. Caricato, A. V. Marenich, J. Bloino, B. G. Janesko, R. Gomperts,
276 B. Mennucci, H. P. Hratchian, J. V. Ortiz, A. F. Izmaylov, J. L. Sonnenberg, D.
277 Williams-Young, F. Ding, F. Lipparini, F. Egidi, J. Goings, B. Peng, A. Petrone, T.
278 Henderson, D. Ranasinghe, V. G. Zakrzewski, J. Gao, N. Rega, G. Zheng, W. Liang,
279 M. Hada, M. Ehara, K. Toyota, R. Fukuda, J. Hasegawa, M. Ishida, T. Nakajima, Y.
280 Honda, O. Kitao, H. Nakai, T. Vreven, K. Throssell, J. A. Montgomery, Jr., J. E.
281 Peralta, F. Ogliaro, M. J. Bearpark, J. J. Heyd, E. N. Brothers, K. N. Kudin, V. N.
282 Staroverov, T. A. Keith, R. Kobayashi, J. Normand, K. Raghavachari, A. P. Rendell,
283 J. C. Burant, S. S. Iyengar, J. Tomasi, M. Cossi, J. M. Millam, M. Klene, C. Adamo,
284 R. Cammi, J. W. Ochterski, R. L. Martin, K. Morokuma, O. Farkas, J. B. Foresman,
285 and D. J. Fox, Gaussian, Inc., Wallingford CT, 2016.
286 39. W. J. van Zeist, F. M. Bickelhaupt, Org. Biomol. Chem. 8 (2010) 3118.
287 40. F. M. Bickelhaupt, J. Comput. Chem. 20 (1999) 114.
288 41. L. Tian, Multiwfn: A Multifunctional Wavefunction Analyzer (version 3.1), 2015.
289 Available from: <http://Multiwfn.codeplex.com> (accessed May 22).
290 42. (a) K. Kitaura, K. Morokuma, Int. J. Quantum Chem 10 (1976) 325. (b) T. Ziegler,
291 A. Rauk Theor Chim Acta. 46 (1977) 1. (c) T. Ziegler, A. Rauk, Inorg Chem. 18
292 (1979) 1755.
293 43. M. P. Mitoraj, M. Parafiniuk, M. Srebro, M. Handzlik, A. Buczek, A. Michalak, J
294 Mol Model, 17 (2011) 2337.

295

296

297

298

299

300

301

302 **TOC Graphic**

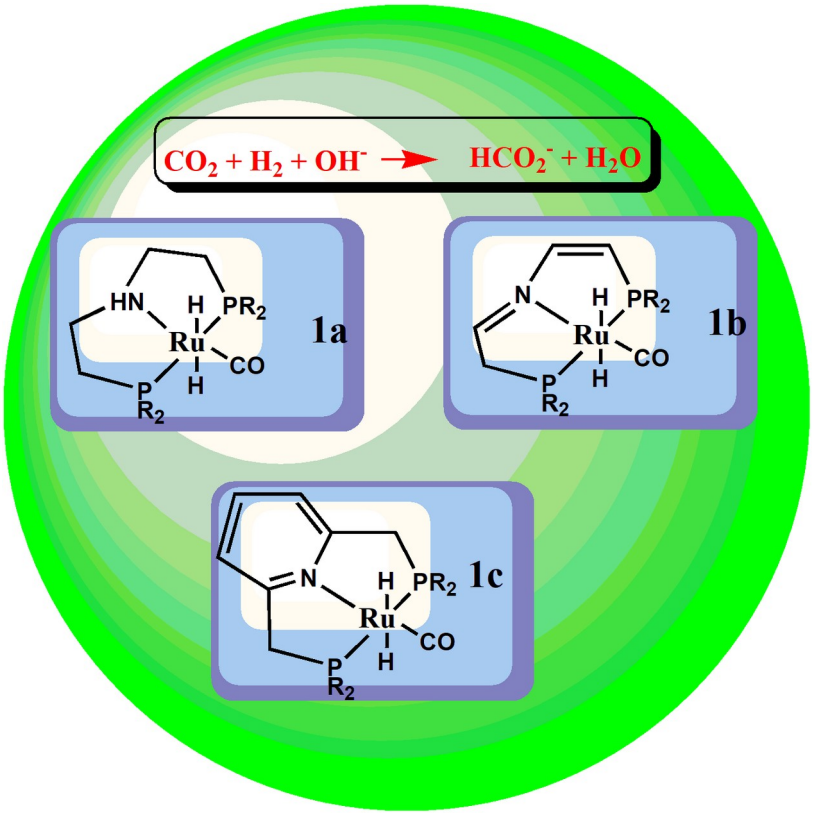

303